Proceedings of "Applications of Physics in Mechanical and Material Engineering" (APMME 2024)

The Impact of Finite Size Effects on the Transmission of Electromagnetic Waves in a Defected, Perforated Waveguide

K.M. Gruszka* and S. Berski

Faculty of Computer Science and Artificial Intelligence, Department of Computer Science, Czestochowa University of Technology, Dąbrowskiego 73, 42-201 Częstochowa, Poland

Doi: 10.12693/APhysPolA.147.280 *e-mail: kgruszka@icis.pcz.pl

This study investigates the impact of finite size effects on the transmission of electromagnetic waves through a defected, perforated two-dimensional waveguide. The research focuses on how transmission characteristics are affected by the number of perforations surrounding a point defect. As the number of perforations increases, the waveguide gradually acquires properties similar to those of an ideal photonic crystal. However, unlike the infinite photonic crystals often assumed in theoretical models, our waveguide has finite dimensions, leading to unique boundary effects. The paper outlines the thresholds at which the finite size effects become prominent, analyzing their influence on wave propagation and transmission efficiency. Theoretical analysis is employed to identify critical points where the finite size alters expected outcomes, providing a deeper insight into the practical limitations and design potential of photonic waveguide-based devices.

topics: finite-difference time-domain (FDTD), waveguide, electromagnetic (EM) transmission

1. Introduction

Waveguides are a key element in technologies related to electromagnetic wave propagation, from optical communication to microwave devices [1–4]. One of the important research aspects in this field is the influence of the size and geometry of waveguides on their transmission properties and band [5]. In particular, perforated waveguides with material defects are becoming the subject of intensive research, because they offer the possibility of controlling wave propagation by precisely adjusting geometric and material parameters [6–9]. Perforations introduced into waveguides allow for the manipulation of electromagnetic waves, enabling selective transmission in selected frequency ranges, which finds application in filters, sensors, and scattering control structures. Adding defects to such structures allows for local modification of band properties, which can be used to design advanced photonic components.

Here, special attention is paid to the finite size effects in a perforated waveguide with a defect. Such a defect is based on a disruption in the continuity of the electric field permittivity by the local introduction of a material with different parameters. This, in turn, leads to a change in the local dispersion of electromagnetic waves and can result in the formation of localized modes within the waveguide. Such structures are analogous to photonic crystals, where the band transmission properties result from a periodic modulation of the refractive index [10, 11]. The aim of this study is to analyze the influence of the number of perforations and the resulting size of the waveguide on the electromagnetic transmission and the band structure. In particular, the authors focus on determining how a local material change affects these properties in a finite length waveguide. The results can serve as a basis for the design of more efficient waveguides with regard to applications in photonic and microwave engineering, as well as for various applications in communication systems, sensors, and other electronic devices.

2. Computational details

Finite-difference time-domain (FDTD) is one of the most commonly used tools for simulating electromagnetic wave propagation in complex structures [12, 13]. Its popularity stems from the direct implementation of Maxwell's equations in discrete form, which allows for modeling the time–space evolution of the electromagnetic field in materials with different properties.

The basic Maxwell equations in the form used in the FDTD method express the dependence of the electric field variables $\boldsymbol{E}$ and magnetic field $\boldsymbol{H}$ as follows

$$\frac{\partial \boldsymbol{E}}{\partial t} = \frac{1}{\epsilon}(\nabla \times \boldsymbol{H}) - \frac{\sigma}{\epsilon}\boldsymbol{E}, \quad (1)$$

$$\frac{\partial \boldsymbol{H}}{\partial t} = -\frac{1}{\mu}(\nabla \times \boldsymbol{E}), \quad (2)$$

where ϵ is the electric permittivity, μ is the magnetic permittivity, and σ is the electrical conductivity.

The FDTD algorithm is based on the discretization of space and time, using the Yee grid, which allows for separate calculation of the $\boldsymbol{E}$ and $\boldsymbol{H}$ fields in successive time steps. The advantages of the FDTD method include the ability to model nonlinear and anisotropic materials and the analysis of dispersion and losses in periodic structures. The main FDTD discretization in the form of Maxwell's equations is expressed as

$$E_x^{n+1}(i,j,k) = E_x^n(i,j,k) - \frac{\sigma \Delta t}{\epsilon} E_x^n(i,j,k)$$
$$+ \frac{\Delta t}{\epsilon}\left[\frac{H_z^n(i,j+\frac{1}{2},k) - H_z^n(i,j-\frac{1}{2},k)}{\Delta y}\right.$$
$$\left. - \frac{H_y^n(i,j,k+\frac{1}{2}) - H_y^n(i,j,k-\frac{1}{2})}{\Delta z}\right], \quad (3)$$

$$H_x^{n+1/2}(i+1/2,j,k) = H_x^{n-1/2}(i+\frac{1}{2},j,k)$$
$$- \frac{\Delta t}{\mu}\left[\frac{E_z^n(i+\frac{1}{2},j+1,k) - E_z^n(i+\frac{1}{2},j,k)}{\Delta y}\right.$$
$$\left. - \frac{E_y^n(i+\frac{1}{2},j,k+1) - E_y^n(i+\frac{1}{2},j,k)}{\Delta z}\right], \quad (4)$$

where n is the time index; i,j,k — spatial indices of the grid; Δt — time step; Δx, Δy, Δz — spatial steps in x,y,z directions; ϵ — electrical permittivity; μ — magnetic field permeability; σ — electric field conductivity.

The simulation domain consists of a two-dimensional waveguide with permittivity of ϵ_w=11.8 immersed in an environment of $\epsilon_a = 1$. The entire cell is surrounded by an absorbing perfectly matched layer (PML), the thickness of which is selected to minimize the reflection of electromagnetic waves towards the waveguide. The computational domain schematic is shown in Fig. 1. All calculations were performed using the Meep package, in which, because the speed of light is set to $c = 1$, frequency units are dimensionless and are expressed in reciprocal of the normalized length. A Gaussian pulse source with a central frequency of $F_g = 1$ with the spread of ± 0.15 was placed within the waveguides to investigate the frequency response of both defective and pristine waveguides. This corresponds to the near-infrared range (NIR). Then, the waveguide length was systematically increased from 14, 18, 24, 28 to 32 μm, which corresponded to a total number of perforations N of 10, 15, 20, 25, and 30. Exactly in the middle of the waveguide, a defect ($\epsilon_d = 5$) was placed, with geometric dimensions identical to the perforations ($r = 0.2\mu m$).

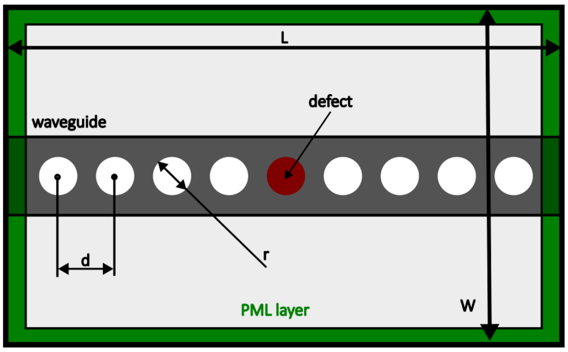

Fig. 1. Schematic diagram of the computational domain, where $d = 1$, $r = 0.2$, $W = 4.8$, width of waveguide $W_w = 1.2$ μm, and length L varies with increasing perforation number.

3. Results and discussion

In Fig. 2, transmission spectra for waveguides with varying perforation numbers without defects are presented. Instead of a central defect, a continuation in perforations is preserved. The figure shows the dependence of the electromagnetic wave transmission (in normalized form, expressed in percentage) on the frequency expressed in units of $2\pi c/a$, for waveguides with different numbers of perforations N (11, 16, 20, 26, 31). The lines represent the results for different values of N, and the continuous line (black) shows the reference transmission characteristic for the waveguide without defect. As the number of perforations increases, a clear reduction in transmission is observed. This is in line with expectations, since a larger number of perforations increases the system loss and its impact on electromagnetic wave propagation. The positions of the main transmission minima and maxima remain largely constant regardless of the number of perforations. This indicates that the waveguide band structure is stable with respect to the number of perforations, and the changes are primarily related to the transmission amplitude. Moreover, the transmission spectrum shows clearly defined minima and maxima, demonstrating the presence of resonances and effects related to the interaction of the wave with the waveguide geometry. Also, transmission characteristics for the waveguide without defect ($N = 11$ treated as a reference case) show clearly higher transmission values, especially in the lower frequency range. For larger N, the

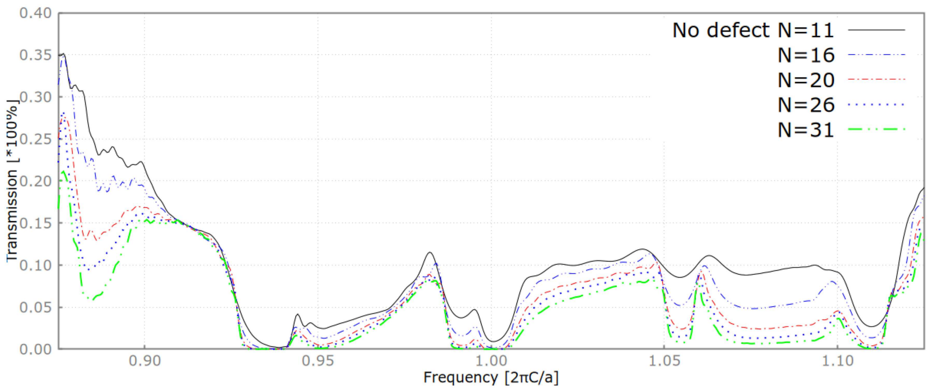

Fig. 2. Transmission spectrum for ideal waveguide structures with a varying number of perforations N without a defect. The transmission values are presented relative to the flat, non-perforated waveguide.

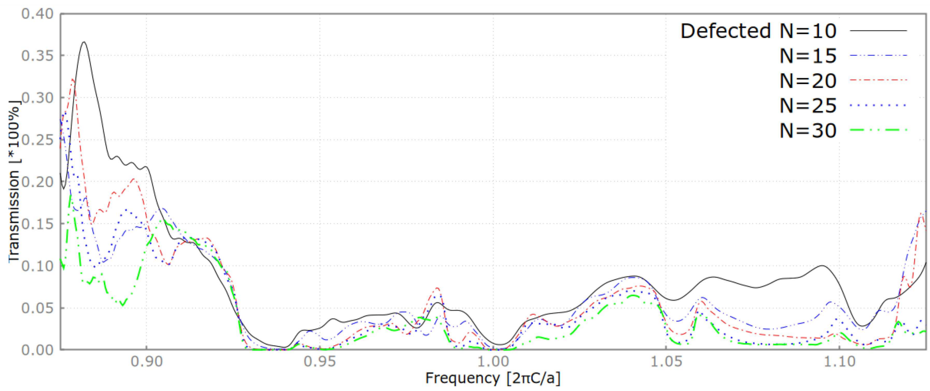

Fig. 3. Transmission spectrum for non-ideal waveguide structures with a varying number of perforations N with a defect in the center. The transmission values are presented relative to the flat, non-perforated waveguide.

transmission amplitude decreases, but the frequency characteristic (position of maxima and minima) is close to that of the reference case.

Next, a similar analysis was performed for the situation in which a defect was introduced into the structure. In Fig. 3, the dependence of electromagnetic wave transmission on frequency in a perforated waveguide is shown. A waveguide defect was introduced, replacing one of the perforations with a material with a different electrical permittivity coefficient ($\epsilon = 5$). The number of perforations N in each analyzed structure was reduced by 1 compared to the structure without a defect, which is included in the designations ($N = 10$, 15, 20, 25, 30). The presence of a defect notably affects the transmission. Compared to a waveguide without a defect, new features appear in the frequency response, such as a shift or modification of transmission maxima and minima (visible especially at the beginning and end of the spectrum). The defect also causes larger changes in the transmission amplitude in some frequency ranges (near 1.00 $2\pi C/a$), which indicates a stronger interaction of the electromagnetic wave with the local change in material properties. As in the case of the defect-free structure, increasing the number of perforations (N) causes an overall decrease in transmission. This is due to the increased losses in the structure and the more complicated interaction of the wave with the larger number of perforations. Nevertheless, the positions of the main transmission minima and maxima remain relatively stable, suggesting that the influence of the defect mainly concerns local effects near the site of the modified perforation insertion. In the range of $f \approx 0.95$, the transmission still drops to very low values, similar to the structure without the defect. More visible differences in transmission appear in the area of $f \approx 1.0$ and $f \approx 1.1$, depending on the number of perforations, which may be the effect of stronger dispersion in the presence of the defect. Compared to the structure without the defect, it is noticeable that local disturbances are introduced in the transmission characteristic. In particular, the transmission amplitudes change in selected frequency ranges.

Figure 4 shows the spatial distribution of the electric component E_z of the electromagnetic field in a defect-free waveguide consisting of $N = 10$ perforations. The positions of the holes are marked with green circles, and the colors on the map indicate

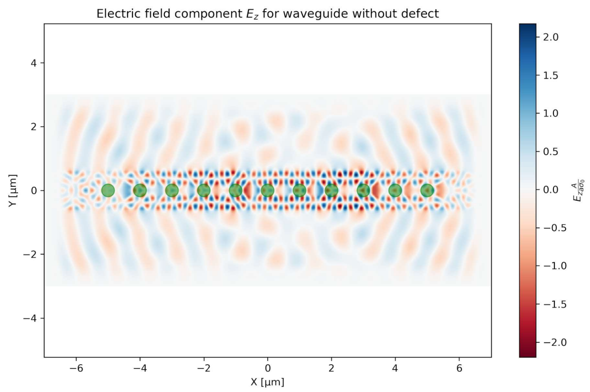

Fig. 4. Distribution of the electric component E_z of the electromagnetic field in the perfect waveguide and in its immediate vicinity for $N = 10$ perforations (green round markers).

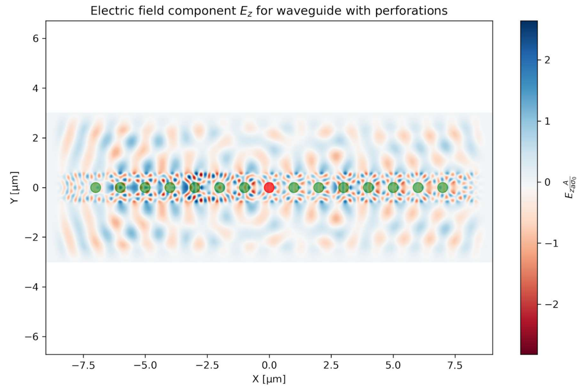

Fig. 5. Distribution of the electric component E_z of the electromagnetic field in the defected (red round marker) waveguide and in its immediate vicinity for a waveguide with $N = 15$ perforations (green round markers).

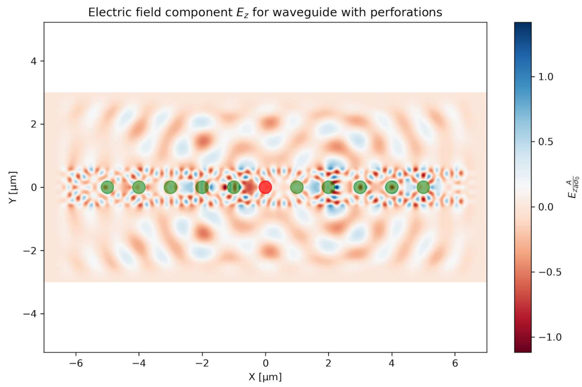

Fig. 6. Distribution of the electric component E_z of the electromagnetic field in the defected (red round marker) waveguide and in its immediate vicinity for a waveguide with $N = 10$ perforations (green round markers).

the values of the E_z component, according to the legend (blue areas correspond to positive values, red to negative values). The electric field distribution E_z is almost symmetrical about the y axis and also demonstrates symmetric features on the second axis. The symmetry indicates that the waveguide geometry and material do not introduce significant interferences to wave propagation in this case. By analyzing this image, it can be seen that the electromagnetic fields are particularly strongly concentrated near the perforations (green circles) and in the area between the perforations and the waveguide boundaries. In these places, local resonances and field scattering occur, which affects the propagation characteristics. Outside the waveguide region, the E_z field values are much smaller, indicating an effective concentration of electromagnetic energy in the waveguide region. The periodic nature of the electric field distribution along the x axis is visible, which results from the interference of the electromagnetic wave within the periodic structure of the waveguide.

In the case of $N = 15$, the symmetry about the y axis is largely preserved, similarly to $N = 10$, but the influence of the defect is more local and less intense. The field pattern around the perforations outside the defect region is more ordered than in the case of $N = 10$. This indicates a greater influence of the structure periodicity on the wave propagation in the case of a larger number of perforations. Compared to $N = 10$, the structure shown in Fig. 5 shows that increasing the number of perforations reduces the effect of the defect on the field distribution, and the structure becomes more periodic and homogeneous.

Figure 6 shows the spatial distribution of the electric component E_z of the electromagnetic field for a perforated waveguide with $N = 10$ perforations, with one perforation replaced by a material with a different coefficient of $\epsilon = 5$. The location of this defect is marked with a red circle, while the other perforations are marked with green circles. The introduction of the defect leads to noticeable changes in the local electromagnetic field distribution near the red circle. The fields around the defect are clearly more concentrated compared to the symmetric distribution in the case of the waveguide without the defect. Despite the local perturbations, the overall symmetry of the field distribution about the $y = 0$ axis is largely preserved, indicating that the defect mainly affects local resonances. It can be seen that the defect introduces disturbances in the periodic nature of the field distribution, causing local shifts in the nodes. These disturbances indicate a change in the propagation conditions of waves near the defect, but the fields are still concentrated near the perforations. The intensity of these interactions is slightly lower compared to the case without the defect. It can be seen that the defect modifies the flow of electromagnetic energy in the waveguide.

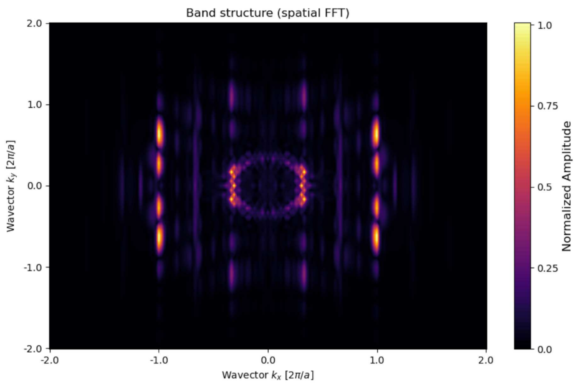

Fig. 7. Two-dimensional k-space band structure for a defect-free waveguide with $N = 10$ perforations, obtained using spatial FFT analysis.

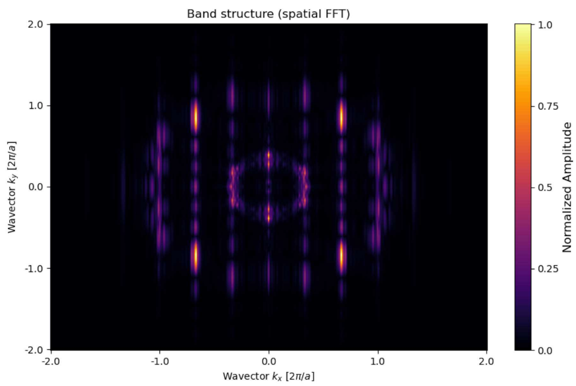

Fig. 10. Two-dimensional k-space band structure for a defected waveguide with $N = 30$ perforations, obtained using spatial FFT analysis.

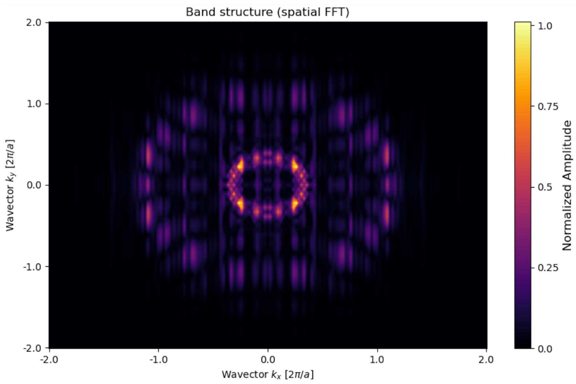

Fig. 8. Two-dimensional k-space band structure for a defected waveguide with $N = 10$ perforations, obtained using spatial FFT analysis.

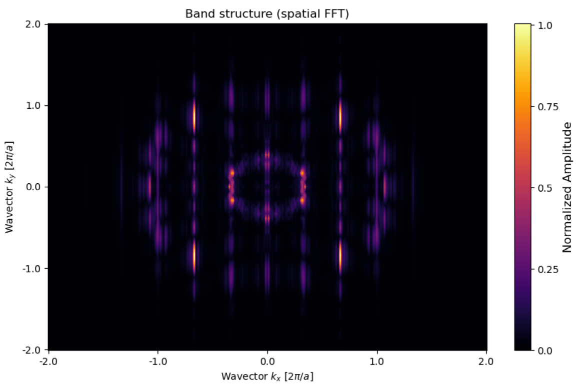

Fig. 9. Two-dimensional k-space band structure for a defected waveguide with $N = 25$ perforations, obtained using spatial FFT analysis.

Increasing the number of perforations to $N = 15$ (Fig. 5) causes a larger field scattering in the whole structure. It can be seen that the field intensity in the defect region (red circle) is lower compared to the waveguide with $N = 10$. The field distribution along the x axis becomes more periodic, indicating a more uniform propagation in the structure with more perforations. This is because the number of perforations increases and the number of defects remains unchanged.

Next, we conducted the Fourier transform analysis (FFT), which allows for the identification of dominant spatial frequencies in the reciprocal space (k_x, k_y) and the characteristics of the symmetry and periodicity of the structures. The two-dimensional Fourier transform of the spatial distribution of the electromagnetic field in perforated waveguide systems is shown in Fig. 7 for a waveguide without a defect ($N = 10$ perforations) and in Figs. 8–10 for waveguides with a centrally introduced defect ($N = 10$, 25, 30 perforations + defect).

The spectrum in Fig. 7 shows high symmetry about the center $(0, 0)$, and the presence of symmetric rings around the center indicates periodic properties of the defect-free system.

In the case of waveguides with a defect, a change in the spectral symmetry is visible. For $N = 10$ (Fig. 8), the symmetry is partially disturbed, especially in the central ring region, which highlights the influence of the local change in the structure (defect) properties. For $N = 25$ (Fig. 9) and $N = 30$ (Fig. 10), the symmetry is more preserved, which may be due to the more dominant influence of the periodicity of the larger number of perforations, which mask the influence of the defect.

In the defect-free structure, distinct concentric rings around the central point indicate well-defined periodicities of the waveguide structure. Bright spots on the rings are proportional to the dominant components of the wave vectors k_x and k_y. In contrast, for the structures with the defect $N = 10$, the central ring is more diffuse, which shows that the defect introduces local perturbations in the periodicity. For $N = 25$, the bright bands around the center start to be better defined compared to the case of $N = 10$, which means that a larger number of perforations restores the dominant periodicities.

When $N = 30$, the bands of the dominant components become more similar to the case without the defect (Fig. 7), which indicates that the influence of the defect decreases in structures with a larger number of perforations.

4. Conclusions

The reduction of transmission with a larger number of perforations is a key effect of the finite size of the waveguide. It is the result of the local interaction of the electromagnetic wave with a larger number of local inhomogeneities introduced by the perforations. The stability of the positions of maxima and minima in the transmission spectrum suggests that the design of such structures can be effective in applications requiring selective wave attenuation while maintaining specific propagation frequencies. The general trend leads to the conclusion that with the increase in the number of perforations, the role of the defect is smaller and smaller. The differences in the spatial FFT character for $N = 25$ and $N = 30$ are much smaller than for the lower number of perforations, and the features present for the first of the mentioned structures are preserved for the second one. This allows us to conclude that for the number of perforations $N = 25$, there is a threshold above which only small changes in the transmission and band structure can be expected for the investigated waveguide, and further changes in the number of perforations will only lead to a reduction in the amplitude of electromagnetic (EM) wave transmission.

Acknowledgments

This research was supported in part by PLGrid Infrastructure.

References

[1] Y.-Q. Wu, M.-Y. Chen, Z.-J. Dai, *Opt. Laser Technol.* **183**, 112339 (2025).

[2] A. Prabhakar, N. Roy, G. Chaudhary, A. Dhwaj, D. Verma, S. Mukherji, *Microchem. J.* **208**, 112508 (2025).

[3] A.J. Alazemi, D. Zarifi, A. Farahbakhsh, *Int. J. Electron. Commun.* **191**, 155692 (2025).

[4] F.Ö. Alkurt, *Int. J. Electron. Commun.* **187**, 155567 (2024).

[5] A. Delitsyn, D.S. Grebenkov, *Appl. Math. Comput.* **412**, 126592 (2022).

[6] X. Zhang, G. Liu, Y. Hu, Z. Liu, Z. Cai, Y. Chen, X. Liu, G. Fu, G. Gu, M. Liu, *Opt. Commun.* **325**, 105 (2014).

[7] K.M. Gruszka, M. Dośpiał, *Acta Phys. Pol. A* **142**, 101 (2022).

[8] E. Andreassen, K. Manktelow, M. Ruzzene, *J. Sound Vib.* **335**, 187 (2015).

[9] M. Dośpiał, K.M. Gruszka, *Acta Phys. Pol. A* **142**, 35 (2022).

[10] O.D.H. Pardo, R.R. Rey-González, *Photon. Nanostruct. Fundam. Appl.* **63**, 101355 (2025).

[11] M. Boulesbaa, B. Mekimah, A. Guermache, *Optik* **322**, 172160 (2025).

[12] L. Cheng, Z. Nianshun, G. Junming, Z. Li, S. Wang, *Optik* **277**, 170664 (2023).

[13] C.S. Mishra, A. Nayyar, S. Kumar, B. Mahapatra, G. Palai, *Optik* **176**, 56 (2019).